The Monte Carlo Method: Versatility Unbounded In A Dynamic Computing World
Chattanooga, Tennessee, April 17–21, 2005, on CD-ROM, American Nuclear Society, LaGrange Park, IL (2005)

MCPTRAN.CAVITY AND MCPTRAN.RZ, MONTE CARLO CODES FOR THE SIMULATION OF PROTON BEAMS AND CALCULATION OF PROTON DETECTOR PERTURBATION FACTORS

Palmans H
National Physical Laboratory
Queens Rd, Teddington TW11 0LW, UK
hugo.palmans@npl.co.uk

ABSTRACT (Abstract Head)

The availability of a growing number of therapeutic proton beams worldwide has invoked increasing interest in the use of the Monte Carlo method to investigate dosimetric characteristics of proton beams and detectors used in these beams.

In this presentation, two proton Monte Carlo user codes are described: McPTRAN.CAVITY for modelling cavities of any shape in a homogeneous slab and McPTRAN.RZ for modelling a two-dimensional voxel geometry in cylindrical coordinates. Both are derived from the Monte Carlo code PTRAN [1] using essentially the same step, multiple scattering and energy loss sampling algorithms. Geometry testing algorithms and scoring procedures were developed independently from the original program and various modifications were applied allowing the simulation of transport in other materials than water, broad beams with various geometrical and energy distributions, transport through inhomogeneities and also dynamic geometries such as a range modulator wheel.

The use of the codes is illustrated with a number of applications and comparisons with experimental results: perturbation correction factors for ionization chambers and solid state detectors, depth dependent response functions of alanine and TLD detectors and modeling of a realistic ocular proton beam line.

Key Words: Proton Beam, Monte Carlo, Dosimetry, Ionization Chamber, Perturbation Factor

1 INTRODUCTION

PTRAN is a class I Monte Carlo code for proton transport in the energy range of clinical proton beams. Its application is restricted to the simulation of pencil beams in homogeneous water and the calculation of depth dose data, radial dose and fluence deposition data and spectral distributions as a function of depth.

We started using this code with the purpose of calculating perturbation factors of various detectors in proton beams in a time that MCNP didn't provide proton transport and GEANT had not developed its low-energy transport modules. To this end, various modifications were applied in the course of many years resulting in a number of codes that essentially use PTRAN's step, multiple scattering and energy loss sampling algorithms, but in which the geometry testing algorithms and scoring procedures were developed independently from the original program. The modifications allow the simulation of transport in other materials than water, broad beams with various geometrical and energy distributions, through cavities, in rz-voxel geometries and also allowed dynamic geometries such as a range modulator wheel. The implementation of the

various adaptations, which resulted in the codes McPTRAN.CAVITY and McPTRAN.RZ, will be described and their use to dosimetry will be illustrated.

2 METHOD

2.1 The original code, PTRAN

PTRAN [1] uses the Monte Carlo method to simulate the transport of proton beams through water. Details on the use of the programs and the methods used in the Monte Carlo transport are given by Berger [1]. A brief summary is given in this section.

The incident proton energies for which the code is designed range from 50 to 250 MeV, although it is applicable to a wider range of energies. PTRAN contains several cross section preparation programs and two main codes, PTRAN3D and PTRAN1D. The code take into account multiple scattering and Coulomb interaction energy loss mechanisms along with non-elastic nuclear interactions. Deposition of energy as a function of depth and radial distance from the beam as well as energy spectra of the primary protons as function of depth are scored.

The simulations follow a class I condensed random walk scheme [2] in which each proton is transported down to a cut-off energy by dividing its track in a series of short steps. They are based on a pre-calculated energy grid at which the various cross section and probability distributions are evaluated. Energy losses in Coulomb collisions with atomic electrons are sampled from the Vavilov energy straggling distribution [3] using the ICRU report 49 stopping powers [4] as average values. Multiple scattering deflections due to elastic scattering by atoms are sampled from the Molière distribution [5]. Energy losses in non-elastic nuclear interactions are based on fits to experimental data from Renberg et al. [6] and Carlson et al. [7] based on theoretical considerations by Seltzer [8].

The scoring algorithm is relatively simple. A set of scoring planes is defined perpendicular to the direction of the incident proton beam. The depths z_i of these planes are defined in terms of the CSDA range r_0. In each plane, an array of concentric radial bins with center (x,y) = (0,0) is defined for the scoring of radial energy deposition distributions as well as an array of energy bins for the scoring of spectra. The positions of the scoring planes and the radial and energy bins are defined in a boundary input file. In the scoring plane, the energy loss per unit depth in Coulomb interactions, $(dE/dz)_C$, is estimated as $S_{cross} \cdot W_{cross}/\cos\theta_{cross}$, the energy loss per unit depth in non-elastic nuclear interactions, $(dE/dz)_N$, is estimated as $E_{cross} \cdot \mu_{cross} \cdot W_{cross}/\cos\theta_{cross}$, and the fluence is estimated as $1/\cos\theta_{cross}$, where E_{cross} is the energy, W_{cross} the fraction of protons that survive without nuclear interaction, survival factor, S_{cross} the stopping power, μ_{cross} the nuclear absorption factor and θ_{cross} the polar angle. The fluence is binned in energy spectra and $(dE/dz)_C$ in the radial bins. Since the energy transferred in non-elastic nuclear interactions is only partially going to charged particles (the rest is escaping through neutrons and photons) this fraction can be taken into account in a post-processing program PTSUM. In this, the energy transferred to secondary charged particles is deposited at the position where they are generated. This is a crude approximation, which is not accurate for high-energy protons where secondary proton disequilibrium has a significant effect on dose distributions.

2.2 McPTRAN.CAVITY – calculation of doses in cavities

In order to enable the simulation of non-water materials and complex non-homogeneous geometries, the code has been changed substantially. Part of these changes have been described by Palmans and Verhaegen [9,10] and are summarized here in brief. For most materials of interest, stopping powers can be taken directly from ICRU report 49 [4]. For materials not listed in there, Bragg's additivity rule can be applied although a recent paper [11] shows that some refinements are required in order to be consistent concerning the calculation of the mean excitation energy I_0 and the Barkas correction. The calculation of the Vavilov distribution require the first moments S_1 and I_1 of the oscillator strength distribution and the mean excitation energies for the calculation of a small correction to the theory introduced by Shulek [12]. S_1 and I_1 were taken from Inokuti et al [13, 14] for all elements with Z ranging from 1 to 38. Bragg's rule was applied for compounds. For the calculation of the Molière multiple scattering distributions, a correction factor k_{HF} has to be applied to the screening angle. These data were taken from Berger and Wang [15]. Non-elastic nuclear interaction cross sections were taken from Janni [16] and ICRU report 63 [17] in the studies described below. For the elements not specified in these references, log-log interpolation of the cross sections as a function of the atomic number was used. In recent work, only the ICRU report 63 data have been considered since they form a more comprehensive set. In addition to the inclusion of data for other materials than water, the range of incident beam types was extended from only mono-directional and mono-energetic beams to circular beams, rectangular beams, beams with an angular distribution and beams with a Gaussian energy distribution.

When a boundary is encountered in a particle's trajectory, the particle is transported to the boundary along the trajectory. The energy loss along the track is scaled with the ratio of the step length up to the boundary to the initially sampled step length. At the boundary, the energy E_{bound}, the polar angle θ_{bound} and the survival factor W_{bound}, are evaluated in the same way as the scoring plane crossing quantities (section 2.1). Given the small scattering angles and energy losses that are involved, we can assume that the errors due to this approximation are small. An evaluation of the influence of the step-cutting artifact revealed no significant effect [10]. For the next step, new multiple scattering angles and energy loss are calculated based on the material properties of the new region.

In the next stage, the original scoring algorithm was abandoned and cylindrical, spherical and thimble cavity geometries were introduced, with the specific purpose of simulating ionization chamber perturbations, hence, this version of the code has been called McPTRAN.CAVITY. Although the scoring planes have no function in the scoring algorithm any more, they proved to be useful for geometry interrogation reduction. In between two of the existing scoring planes a number of non-intersecting and embedded spherical and/or cylindrical cavities can be defined. The situation of a thimble ionization chamber geometry is illustrated in figure 1. A geometry interrogation slab region is defined around the (embedded) cavities representing the ionization chamber. Boundary crossing testing is only performed in this geometry interrogation region. All protons are set in motion on the central axis. Upon reaching the geometry interrogation region the phase space parameters of the proton are stored and history splitting is applied: the proton is set in motion again translated from the beam axis according to coordinates sampled from the geometrical distribution of the incident field. If the lateral distance to the outer cavity is larger than a pre-calculated maximum lateral deflection over the length of the geometry interrogation slab, the history is not simulated, else it is simulated until the distal

edge of the slab is reached. This process is repeated a number of times such that on the average the proton will hit the outer cavity once. If this whole process is finished, the initial history that was started on the central axis is again resumed with the cavity + geometry interrogation region translated to a new depth. This way a depth dose response curve for the ionization chamber can be simulated in one Monte Carlo run. The scoring algorithm works as follows. In each geometrical region, the track length can be scored and binned into an energy spectrum. The boundary-crossing algorithm assumes that track length is distributed evenly along the step. Energy loss is calculated as the difference between the begin and end energy of the step (whether it be a 'normal' or a cut-off step). The non-elastic nuclear energy transfer is scored at the average value of the energies at begin and end of the step. If desired, both quantities in the previous two steps can be binned as a function of energy as well.

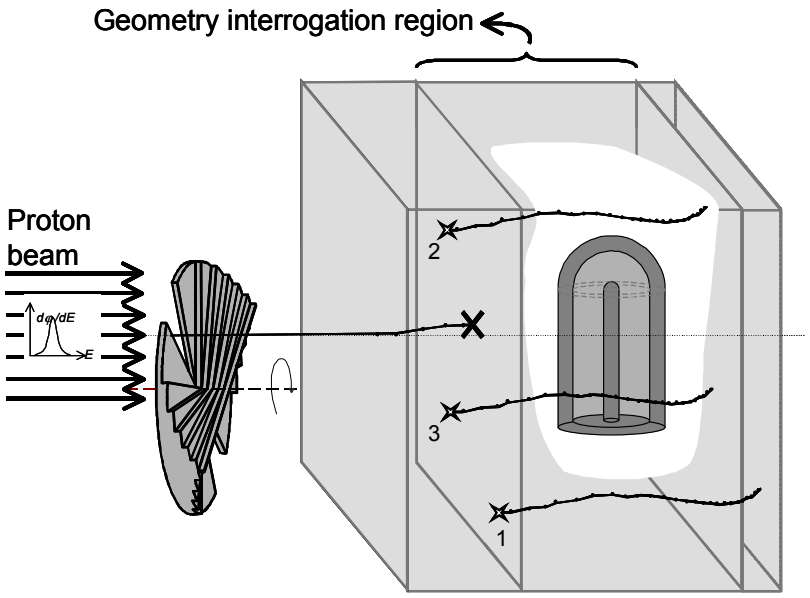

Figure 1. Geometry with dynamic modulator wheel and three concentric thimble cavities representing an ionization chamber as modeled in McPTRAN.CAVITY.

The implementation of a modulator wheel is done by including an additional layer at the front of the geometry. For each incident proton, the thickness of this layer is sampled from the distribution of the wheel thickness. The incident proton is then set in motion at the front of this additional layer. The usual situation where the wheel is a long distance away from the phantom can be easily dealt with by defining the second layer as air with the thickness equaling the distance between the modulator wheel and phantom. The implementation of a modulator wheel in this way is an approximation since the effect of the steps between the different sectors of the real modulator wheel is not taken into account. An example where the full geometry of a modulator is coded is given by Paganetti [18].

2.3 McPTRAN.RZ – calculation of doses in rz-geometry

Departing from the code described in the previous section, the implementation of an rz-voxel geometry is straightforward. The slab geometry is retained and a number of concentric cylinders are constructed perpendicularly to the slabs. In each of the rz-voxels, a different medium can be specified and the same quantities as in McPTRAN.CAVITY can be scored. The geometry is shown in figure 2.

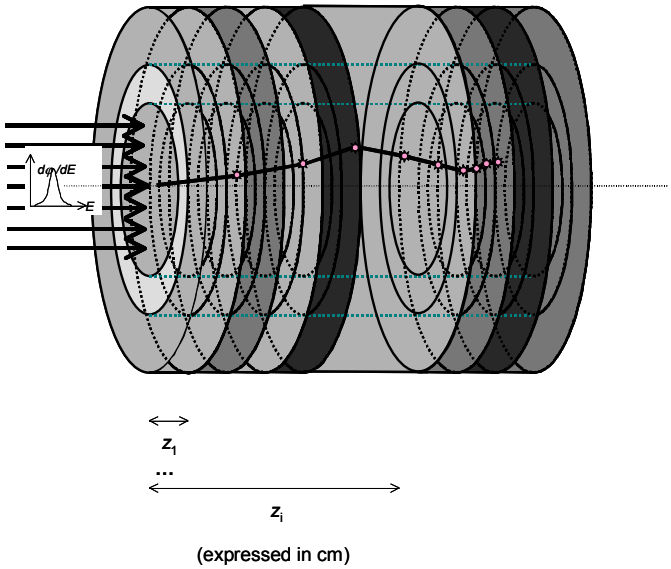

Figure 2. Geometry used in McPTRAN.RZ.

3 APPLICATIONS

3.1 Gradient correction factors for cylindrical ionization chambers

The response of a graphite walled NE2571 ionization chamber was measured as a function of wall thickness in a PMMA phantom. To this end, four graphite build-up caps (serving as sleeves to increase the apparent wall thickness) and corresponding PMMA holders to fit in the phantom were constructed. The thicknesses of the build-up caps were 1.5 mm, 2.5 mm, 4.5mm and 9.5 mm. The measured dose response as a function of wall thickness was compared with Monte Carlo calculated values using McPTRAN.CAVITY. The results, reported in [19], are shown in figure 3. This code was used to calculate the effective point of measurement for a number of ionization chamber types [20-22].

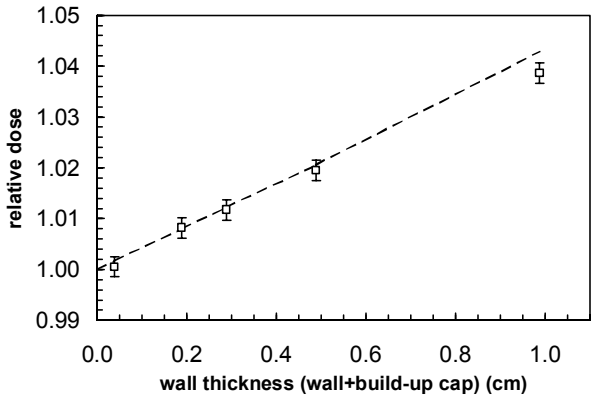

Figure 3. Monte Carlo calculated (dashed line) and measured (symbols) variation of the ionization chamber signal as a function of graphite wall thickness (reproduced from Palmans et al. [19]).

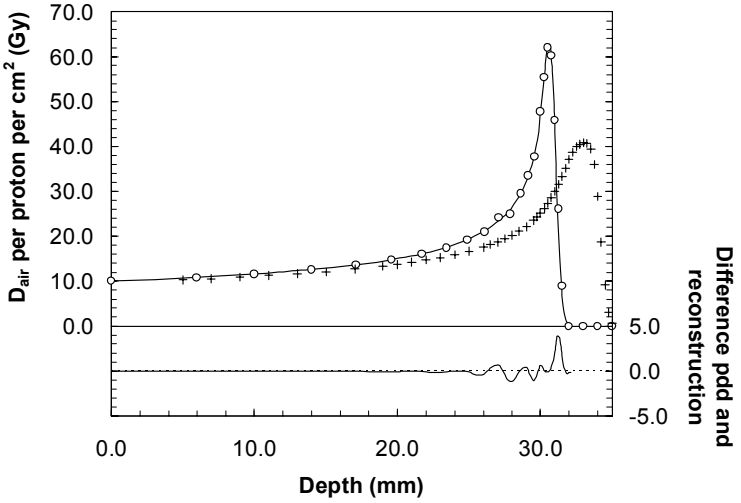

Figure 4. Reconstruction of a depth dose curve from an ionization chamber response for a NE2561 in a 60 MeV mono-energetic proton beam. The + symbols are the result from a Monte Carlo simulation, the full curve is the depth dose curve in homogeneous water and the symbols are the points left as free parameters for the reconstructed depth dose curve. The lower panel gives the difference, expressed as a percentage of the dose maximum, between the cubic spline through the reconstructed data points and the curve in homogeneous water.

Palmans [21,22] developed an analytical model to calculate gradient perturbation effects for cylindrical ionization chambers in proton and heavy ion beams. Tuning parameters in this analytical model in order to give an optimal agreement with the Monte Carlo simulations gives a model that can be used to solve the inverse problem of deriving the depth dose curve in homogeneous water from the depth response curve of the ionization chamber. This is illustrated in figure 4.

The line is the depth dose curve in homogeneous water. The + symbols represent a Monte Carlo simulated response curve for a NE2561cylindrical ionization chamber. The circles represent the reconstructed curve according to the inverse model. The line at the bottom (right hand vertical axis) is the difference between a cubic spline through the symbols and the depth dose curve in homogeneous water. The difference in the distal edge of the Bragg peak exceeds 3% but this corresponds to a very small shift. One must notice that this is an extreme case of a chunky ionization chamber in a low-energy beam, hence the model can be expected to do much better for smaller IC's and at higher-energies.

3.2 Depth dose distributions measured with alanine pellets and TLDs

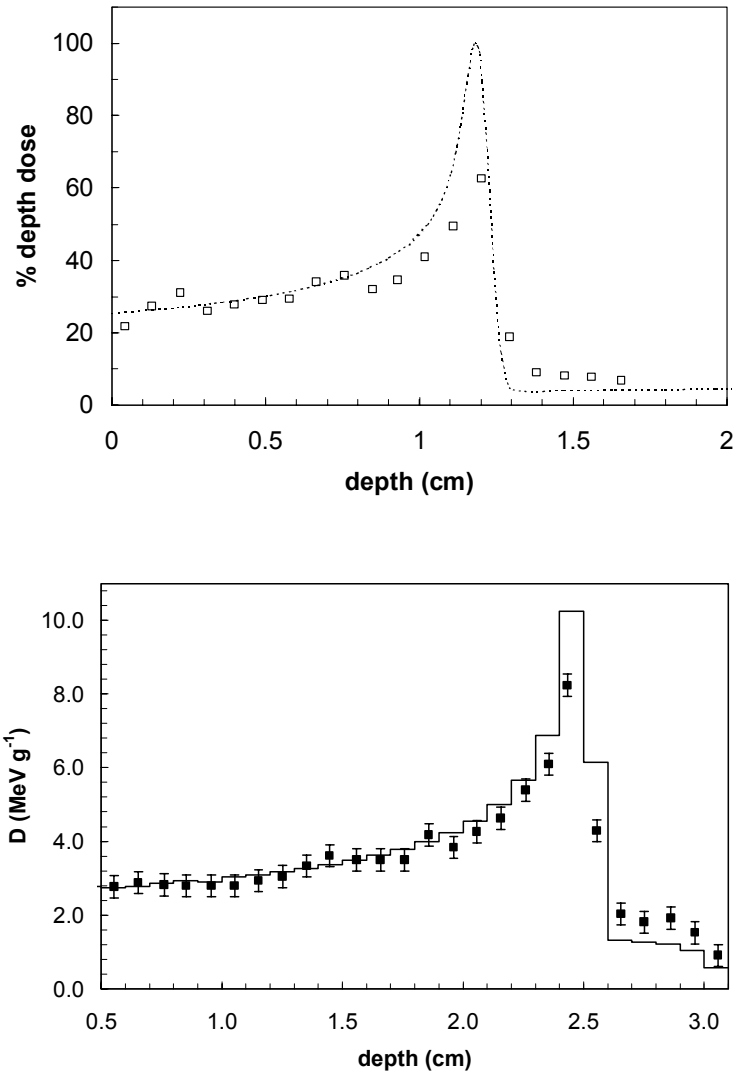

Figure 5. Dose in a stack of TLD pellets (upper) ad a stack of alanine pellets in a PMMA phantom, measured (symbols) by Fattibene et al. [23] for the TLD results and Onori et al [24] for the alanine results and calculated with McPTRAN.RZ using a Gaussian energy distribution with a mean value of 62 MeV and a variance of 0.5% (line).

Figure 5 shows the application to a stack of alanine pellets and a stack of TLDs in a PMMA phantom. These simulations were performed to investigate the source of the tail beyond the Bragg peak. The agreement is fine up to the beginning of the Bragg peak. In the Bragg peak there seems to be an under response of both solid-state dosimeters which is consistent with other results in the literature [11]. The tail in the calculation is the result of in scatter from the surrounding medium and under predicts the effect. The remainder of the measured signal might be due to tunneling of protons through the air gap between the pellets and the PMMA phantom [11,24].

3.3 Modeling of the CCO ocular proton beam line

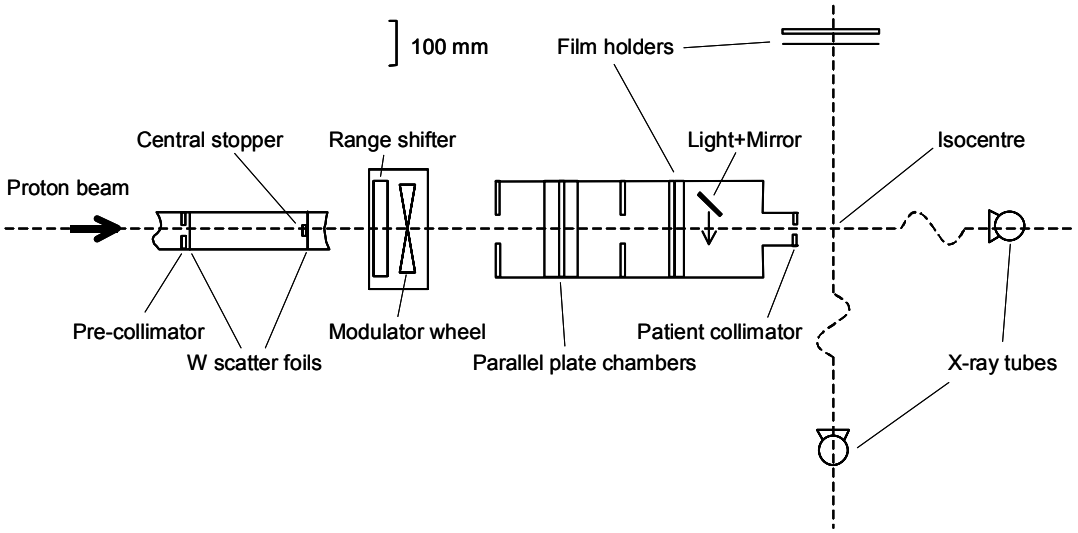

Figure 6 Schematic drawing of the beam line at CCO (Adapted from Bonnet et al. [25])

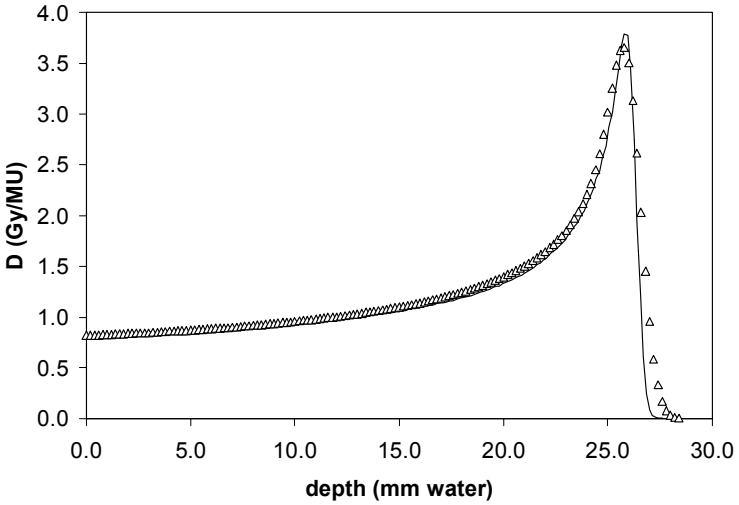

Figure 7. Depth dose curve for the 60 MeV CCO beam line, measured with a diode (full line) and calculated using PTRAN.RZ using an incident energy spread of 1% (symbols).

The CCO beam line has been described in detail by Bonnet et al. [25]. The cylindrical geometry of the beam line has been modelled using PTRAN.RZ and the resulting depth dose curve assuming a variance of the energy spread of 1% is shown in figure 7. The high energy spread was required to reproduce the peak to plateau ratio and results in a Bragg peak width, which is larger than the experimental curve measured with a diode. For lower values of the energy spread the dose maximum was higher than the experimental value. The source of this discrepancy is at present under investigation in collaboration with Baker et al. [26] and Shipley et al. [27].

4 CONCLUSIONS

Two user codes using the transport algorithm of the existing Monte Carlo code PTRAN, McPTRAN.CAVITY and McPTRAN.RZ, have been described. They are able to simulate proton transport in inhomogeneous and complex geometries and beams as well as dynamic modulator wheels. The successful application of these codes for the calculation of gradient corrections of ionization chambers, depth dose response curves of solid-state detectors as TLD and alanine and modeling of proton beam lines has been demonstrated. Future work will include the transport of secondary charged particles form nonelastic nuclear interactions.

5 ACKNOWLEDGMENTS

This work was funded as part of the UK National Measurement System, Ionising Radiation Metrology Programme by the National Measurement System Policy Unit of the UK Department of Trade and Industry.

6 REFERENCES

1. M. J. Berger, “Proton Monte Carlo transport program PTRAN,” *National Institute for Standards and Technology Report* NISTIR 5113, NIST, Gaithersburg, USA (1993).

2. M. J. Berger, “Monte Carlo calculation of the penetration and diffusion of charged particles,” *Methods in computational physics, Vol. 1*, Ed. B. Alder, S. Fernbach and M. Rotenberg, Academic Press, New York, USA (1963).

3. P. V. Vavilov, “Ionization losses of high-energy particles,” *Sov. Phys.-JETP*, **5**, pp.749-751 (1957).

4. ICRU (1993) “Stopping powers and ranges for protons and alpha particles,” *International Commission on Radiation Units and Measurements* Report 49 (Bethesda, USA: ICRU)

5. G. Z. Molière, “Theorie der Streuung schneller geladener Teilchen. II. Mehrfach- und Vielfachstreuung,” *Z. Naturforsch*, **3**, pp.78 – 97 (1948).

6. P. U. Renberg, D. F. Measday, M. Pepin, P. Schwaller, B. Favier and C. Richard-Serre, “Reaction cross sections for protons in the energy range 220-570 MeV,” *Nucl. Phys. A*, **183**, pp.81-104 (1972).

7. R. F., Carlson, A. J., Cox, J. R., Nimmo, N. E., Davison, S. A., Elbakr, J. L., Horton, A., Houdayer, A. M., Sourkes, W. T. H. Van Oers, and D. J. Margaziotis, "Proton total reaction cross sections for the doubly magic nuclei O-16, Ca-40 and Pb-208 in the energy range 20-50 MeV." *Phys. Rev. C*, **12**, pp.1167-1175 (1975).

8. S. M. Seltzer, "An assessment of the role of charged secondaries from nonelastic nuclear interactions by therapy proton beams in water." *National Institute for Standards and Technology Report* NISTIR 5221, NIST, Gaithersburg, USA (1993).

9. H. Palmans and F. Verhaegen, "Calculated depth dose distributions for proton beams in some low-Z materials," *Phys. Med. Biol.*, **42**, pp.1175-1183 (1997).

10. H.Palmans and F. Verhaegen, "Monte Carlo study of fluence perturbation effects on cavity dose response in clinical proton beams," *Phys. Med. Biol.*, **43**, pp.65-89 (1998).

11. H. Palmans, "Effect of alanine energy response and phantom material on depth dose measurements in ocular proton beams," *Technol. Cancer Res. Treat.*, **2**, pp.579-586 (2003).

12. P. Shulek, B. M. Golovin, L. A. Kolyukina, S. N. Medvedev and P. Pavlovich, "Fluctuation of ionization losses," *J. of Nucl. Phys.*, 4, pp.564-566 (in Russian) (1966).

13. M. Inokuti, T. Baer and J. L. Dehmer, "Systematics of moments of dipole oscillator-strength distributions for atoms in the first and second row," *Phys. Rev. A*, **17**, pp.1229-1231 (1978).

14. M. Inokuti, J. L. Dehmer, T. Baer and J. D. Hanson, "Oscillator-strength moments, stopping powers and total inelastic-scattering cross sections of all atoms through strontium," Phys. Rev. A, **23**, pp.95-109 (1981).

15. M. J. Berger and R. Wang, "Multiple-scattering angular deflections and energy-loss straggling," *Monte Carlo Transport of Electrons and Photons*, Ed. T. M. Jenkins, R. Nelson and W. R. Rindi, pp.21 – 56, Plenum Press, New York, USA (1988).

16. J. F. Janni, "Proton range-energy tables, 1 keV - 10 GeV," *Atom. Data Nucl. Data Tables*, **27**, pp.147-339 (1982).

17. ICRU "Nuclear data for neutron and proton radiotherapy and for radiation protection dose," *International Commission on Radiation Units and Measurements* Report 63, ICRU, Bethesda, USA (2000).

18. H. Paganetti, "Four-dimensional Monte Carlo simulation of time dependent geometries," *Phys. Med. Biol.*, **49**, pp.N75-N81 (2004).

19. H. Palmans, F. Verhaegen, J.-M. Denis, S. Vynckier and H. Thierens, "Experimental p_{wall} and p_{cel} correction factors for ionization chambers in low-energy clinical proton beams," *Phys. Med. Biol.*, **46**, pp.1187-1204 (2001).

20. H. Palmans and F. Verhaegen, "On the effective point of measurement of cylindrical ionization chambers for proton beams and other heavy charged particle beams," *Phys. Med. Biol.*, **45**, pp.L20-L22 (2000).

21. H. Palmans, "Analytical expressions for the determination of the effective water depth of an ionization chamber for clinical proton beam dosimetry," CD-ROM Proceedings of the World

Congress on Medical Physics and Biomedical Engineering Chicago, USA, July 23-28 2000, 4 pp (2000).

22. H. Palmans, "Perturbation factors for cylindrical ionisation chambers in proton beams: I. Corrections for gradients," *Phys. Med. Biol.*, submitted (2005).

23. P. Fattibene, A. Calicchia, F. d'Errico, C. DeAngelis, E. Egger and S. Onori, "Preliminary assessment of LiF and alanine detectors for the dosimetry of proton therapy beams," *Radiat. Prot. Dosim.*, **66**, pp.305-309 (1996).

24. S. Onori, F. d'Errico, C. De-Angelis, E. Egger, P. Fattibene and I. Janovsky, "Alanine dosimetry of proton therapy beams," *Med. Phys.*, **24**, pp.447-453 (1997).

25. D. E. Bonnett, A. Kacperek, M. A. Sheen and T. E. Saxton, "The 62 MeV proton beam for the treatment of ocular melanoma at Clatterbridge," *Br. J. Radiol*., **66**, pp.907-914 (1993).

26. C. Baker, A. Kacperek and H. Palmans, "Monte Carlo simulation of a clinical 60 MeV proton beam line," Abstracts of the 40th meeting of the Proton Therapy Co-Operative Group (PTCOG), Paris, 15-18 June 2004.

27. D. Shipley, H. Palmans, C. Baker and A. Kacperek, "GEANT4 simulation of an ocular proton beam and benchmark against other Monte Carlo codes," Monte Carlo 2005 Topical meeting, Chattannooga, USA, 17-21 April 2005 (this conference).